### References

BOER, J. L. DE & DUISENBERG, J. M. (1984). *Acta Cryst.* A**40**, C-410.

CHIANELLI, R. R., SCANLON, J. C. & THOMPSON, A. H. (1975). *Mater. Res. Bull.* **10**, 1379–1382.

GOTOH, Y., GOTO, M., KAWAGUCHI, K., OOSAWA, Y. & ONODA, M. (1990). *Mater. Res. Bull.* **25**, 307–314.

JANNER, A. & JANSSEN, T. (1980). *Acta Cryst.* A**36**, 408–415.

KATO, K. (1990). *Acta Cryst.* B**46**, 39–44.

MAKOVICKY, E. & HYDE, B. G. (1981). *Struct. Bonding (Berlin)*, **46**, 101–170.

MEETSMA, A., WIEGERS, G. A., HAANGE, R. J. & DE BOER, J. L. (1989). *Acta Cryst.* A**45**, 285–291.

ONODA, M., KATO, K., GOTOH, Y. & OOSAWA, Y. (1990). *Acta Cryst.* B**46**, 487–492.

PETŘÍČEK, V. & COPPENS, P. (1988). *Acta Cryst.* A**44**, 235–239.

PETŘÍČEK, V., MALY, K., COPPENS, P., BU, X. CISAROVA, I. & FROST-JENSEN, A. (1991). *Acta Cryst.* A**47**, 210–216.

SMAALEN, S. VAN (1989). *J. Phys. Condens. Matter*, **1**, 2791–2800.

SMAALEN, S. VAN (1991*a*). *Phys. Rev. B.* In the press.

SMAALEN, S. VAN (1991*b*). *J. Phys. Condens. Matter*, **3**. In the press.

SPEK, A. L. (1982). *Computational Crystallography*, edited by D. SAYRE, p. 528. Oxford: Clarendon Press.

WIEGERS, G. A., MEETSMA, A., HAANGE, R. J., VAN SMAALEN, S., DE BOER, J. L., MEERSCHAUT, A., RABU, P. & ROUXEL, J. (1990). *Acta Cryst.* B**46**, 324–332.

WIEGERS, G. A., MEETSMA, A., VAN SMAALEN, S., HAANGE, R. J. & DE BOER, J. L. (1990). *Solid State Commun.* **75**, 689–692.

WIEGERS, G. A., MEETSMA, A., VAN SMAALEN, S., HAANGE, R. J., WULFF, J., ZEINSTRA, T., DE BOER, J. L., KUYPERS, S., VAN TENDELOO, G., VAN LANDUYT, J., AMELINCKX, S., MEERSCHAUT, A., RABU, P. & ROUXEL, J. (1989). *Solid State Commun.* **70**, 409–413.

WOLFF, P. M. DE, JANSSEN, T. & JANNER, A. (1981). *Acta Cryst.* A**37**, 625–636.

WULFF, J., MEETSMA, A., VAN SMAALEN, S., HAANGE, R. J., DE BOER, J. L. & WIEGERS, G. A. (1990). *J. Solid State Chem.* **84**, 118–129.


*Acta Cryst.* (1991). B**47**, 325–333

# Caesium Substitution in the Titanate Hollandites $Ba_xCs_y(Ti^{3+}_{y+2x}Ti^{4+}_{8-2x-y})O_{16}$ from 5 to 400 K


BY ROBERT W. CHEARY

*School of Physical Sciences, University of Technology Sydney, PO Box* 123, *Broadway, New South Wales, Australia* 2007


(*Received* 30 *August* 1990; *accepted* 8 *January* 1991)


## Abstract

Neutron powder diffraction data were collected for the titanate hollandites $Cs_{1\cdot36}Ti_8O_{16}$, $Cs_{0\cdot82}Ba_{0\cdot41}Ti_8O_{16}$ and $Cs_{0\cdot40}Ba_{0\cdot79}Ti_8O_{16}$ over the temperature range 5 to 400 K. Rietveld refinement was used to determine the tetragonal lattice parameters and the structural parameters of these compounds. The lattice parameters $a$ and $c$ increase with Cs concentration from $a = 10\cdot1688\,(2)$ and $c = 2\cdot9595\,(1)$ Å in $Cs_{0\cdot40}Ba_{0\cdot79}Ti_8O_{16}$ at 5 K to $a = 10\cdot2682\,(2)$ and $c = 2\cdot9643\,(1)$ Å in $Cs_{1\cdot36}Ti_8O_{16}$ at the same temperature. The expansion in these compounds is isotropic only in $Cs_{1\cdot36}Ti_8O_{16}$ with a linear-expansion coefficient of $\sim 8 \times 10^{-6}\,K^{-1}$ at 300 K. The presence of Cs is evident by the compression of the centres of the oxygen octahedral walls separating adjacent tunnels and by the enlargement of the tunnel cross-section. It is evident that the mean ⟨Ti—O⟩ bond length in the oxygen octahedra is influenced not only by the relative $Ti^{3+}/Ti^{4+}$ concentration in the octahedra but also by the Cs in the tunnels. The oxygen box forming the cavity around each tunnel ion, Ba or Cs, is approximately 10% larger in $Cs_{1\cdot36}Ti_8O_{16}$ than in the pure Ba hollandite $Ba_{1\cdot07}Ti_8O_{16}$. All the tunnel ions are off-centred along the tunnel directions owing to the large size of Cs in relation to the intrinsically small tunnel cavities and the pairing of these ions in the tunnels. Positional disorder of all the ions is evident in the temperature factors, which possess a large temperature-independent component. The X-ray Debye temperature $\theta_M$ of each hollandite is in the range 420 to 460 K and the r.m.s. displacement of the tunnel ions along the tunnel axis arising from positional disorder is between 0·16 and 0·20 Å. In the context of hollandites being used as hosts for radioactive Cs in nuclear waste, an analysis is presented of the possibilty of Cs or Ba migration along the tunnels.


## Introduction

A key aspect of the development of a solid wasteform for high-level nuclear waste is the immobilization of radioactive caesium. This element constitutes a major component of nuclear waste and is normally associated with extremely soluble compounds rather than chemically inert compounds. In the titanate wasteform known as SYNROC (Fielding & White, 1987) caesium is immobilized quite successfully with a leach resistance many orders of magni-

0108-7681/91/030325-09$03.00

tude higher than glass wasteforms particularly at high temperatues (Cheary, 1988). Within this matrix caesium is captured in solid solution by the barium hollandite phase forming a hollandite with the unit-cell composition $Ba_xCs_y([Ti/Al]^{3+}_{2x+y}Ti^{4+}_{8-x-2y})O_{16}$. In this compound Ba and Cs share the tunnel sites of the structure whilst the titanium and aluminium ions go into oxygen octahedral sites within the tunnel walls. In the absence of $Ti^{3+}$ ions, Cs substitution in Ba hollandite is limited to approximately 0·3 Cs per cell (Cheary, 1987) although more can be squeezed in under hydrothermal preparation conditions (Roth, 1981). This limitation arises from the large size of $Cs^+$ ($R \simeq 1{\cdot}75$ Å) and the fact that the tunnel sites in $Ba_{1\cdot14}[Al_{2\cdot28}Ti_{5\cdot72}]O_{16}$ can only accommodate ions with a radius $< 1{\cdot}5$ Å without developing localized distortions. Above 0·3 Cs per cell the structure is metastable because a significant proportion of Cs ions will be forced to have other Cs ions as nearest neighbours rather than a vacancy or a Ba ion thereby imposing an unacceptable level of deformation in the tunnels.

When reducing conditions are imposed on the starting materials, it is possible to substitute all the Ba with Cs up to 1·5 Cs per unit cell (Kesson & White, 1986*a*,*b*). In these hollandites some of the $Ti^{4+}$ in the tunnel walls are reduced to $Ti^{3+}$ ions and when this occurs the tunnel walls expand creating tunnel sites large enough to accommodate Cs (Cheary, 1990). Of all the hollandites of the type $Ba_x(M_yTi^{4+}_{8-y})O_{16}$ those with $M = Ti^{3+}$ have the largest lattice parameters and, as a consequence, the largest tunnel sites. Kesson & White (1986*a*,*b*) have identified the compositions that exist in the solid-solution series $Ba_xCs_y([Ti/Al]^{3+}_{2x+y}Ti^{4+}_{8-x-2y})O_{16}$. Hollandites without Cs and Al are monoclinic (space group *I*2/*m*) and form over the composition range $Ba_{1\cdot07}Ti_8O_{16}$ to $Ba_{1\cdot33}Ti_8O_{16}$. When the temperature is raised all this group of hollandites can be converted to tetragonal *I*4/*m* ($T_c = 375$ K for $x = 1{\cdot}07$ and 475 K for $x = 1{\cdot}31$) but on cooling through these transitions it is possible for both the tetragonal and monoclinic phases to coexist even down to 5 K. Between these titanate hollandites and the barium aluminous hollandites $Ba_xAl^{3+}_{2x}Ti^{4+}_{8-2x}O_{16}$ [$1{\cdot}14 \leq x \leq 1{\cdot}23$ (Cheary, 1986)] the symmetry changes from monoclinic to tetragonal. The addition of approximately 0·1 Cs per cell to the monoclinic titanate is sufficient to induce the transformation to a tetragonal hollandite. This occurs because the large Cs ions prevent the tunnel walls collapsing onto the tunnel ions (Cheary, 1987). According to Kesson & White (1986*a*,*b*), up to 1·33 Cs per cell can be incorporated in titanate hollandites (*viz.* $Cs_{1\cdot33}Ti_8O_{16}$) but when a small proportion of Al is present along with $Ti^{3+}$, this can be extended to 1·5 Cs.

The general purpose of the present study is to investigate how the crystal structure of titanate hollandites adapts to changes in temperature and the gradual replacement of Ba by Cs (*viz.* $Ba_xCs_yTi_8O_{16}$). It is of central importance to the SYNROC program to understand how Cs is accommodated and what factors limit the stability of these ions on the tunnel sites. The first part of this work on Ba hollandites $Ba_xTi_8O_{16}$ ($x = 1{\cdot}07$ and 1·31) over the temperature range 5 to 500 K has already been published (Cheary, 1990). In the present paper three single-phase, polycrystalline titanate hollandites containing different levels of Cs up to a pure Cs hollandite are investigated over the temperature range 5 to 400 K using high-resolution neutron powder diffraction data. Rietveld refinement is employed to determine both the lattice and structural parameters of these hollandites.

## The hollandite structure

The hollandites considered in this paper are all tetragonal with the space group *I*4/*m* and lattice parameters $a \simeq 10$ and $c \simeq 3$ Å. This structure contains two distinct features; *c*-axis tunnels occupied by the Ba and Cs, and four tunnel walls per tunnel formed from oxygen octahedra which in this instance enclose the $Ti^{3+}$ and $Ti^{4+}$ ions. A (001) projection of a hollandite extended over a number of unit cells is shown in Fig. 1 along with a diagram which defines the various positions within the basic units of this

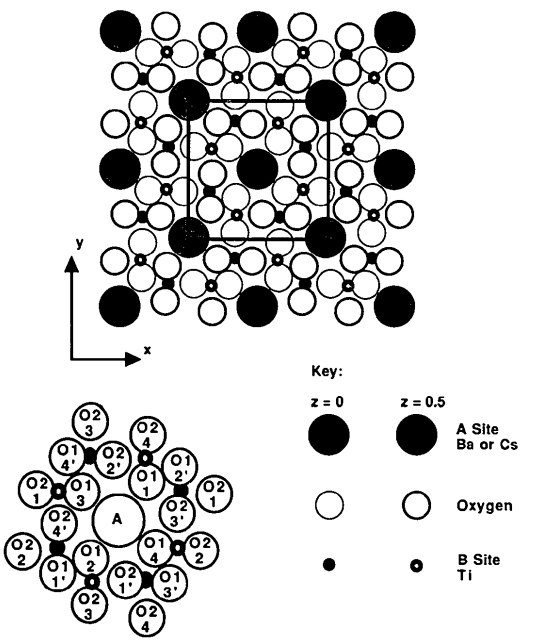


Fig. 1. Projection of the hollandite structure looking down the tunnel axis defining the unit cell (within the bold square) and the nomenclature used to describe the oxygen positions.

structure. In terms of available sites, each unit cell has the composition $A_2B_8O_{16}$ where $B$ represents Ti sites in the oxygen octahedra and $A$ are the tunnel sites which are only partially occupied by Cs and Ba. The $A$ site occupancy in these compounds can vary from 57% in $Ba_{1.14}Ti_8O_{16}$ up to 67% in $Cs_{1.33}Ti_8O_{16}$ but has been known to reach 75% in K and Rb hollandites and even Cs hollandites containing a small proportion of $Al^{3+}$ alongside $Ti^{3+}$. In tetragonal hollandites all the O octahedra are the same size but slightly distorted and the $B$ ions within them are off-centre because of the electrostatic repulsion between adjacent columns of $B$ ions. The O octahedra are bonded together by edge sharing within the walls and the walls themselves are tied by corner sharing. During the monoclinic–tetragonal transformation these corner shared oxygens act as hinges along the $c$ axis allowing the tunnel cross-section to change from a rhombus to a square without significant deformation of the tunnel walls. Each $A$ site is surrounded by a box of eight oxygens formed from two square-planar arrays of the oxygens $O1_1$—$O1_4$—$O1_2$—$O1_3$ above and below the $A$ site in the tunnel-axis direction. Ordering usually occurs amongst the Ba, Cs and vacant $A$ sites which shows up as superlattice lines in the X-ray or electron diffraction pattern (Bursill & Grzinic, 1980). At 67% occupancy the ordered structure has a repeat of $3c$ along each tunnel, where $c$ is the hollandite tunnel-axis lattice parameter, and the filled ($F$) and vacant ($V$) sites follow the pattern [$FFV$]–[$FFV$]–... The pairing of filled sites in this arrangement creates a mutual electrostatic repulsion and these ions assume an off-centre position within their oxygen boxes. In the context of nuclear-waste disposal the size of the square-planar array of oxygens in relation to the size of a Ba or Cs ion and the pressure imposed on this array by the off-centring forces are important factors in determining the migration energy of these cations and the general stability of the hollandite structure particularly when the material is subject to radiation damage.

## Specimen preparation, measurement and refinement procedures

Three hollandite specimens each of about 12 g were prepared for neutron diffraction studies all with Ti ions only on the $B$ sites but with differing proportions of Cs and Ba on the $A$ sites: one with Cs only, one with $\frac{2}{3}$Cs + $\frac{1}{3}$Ba and the other with $\frac{1}{3}$Cs + $\frac{2}{3}$Ba. To make up these samples it was assumed that the total occupancy and the Cs content on the $A$ sites are linearly related between the end members $Ba_{1.14}Ti_8O_{16}$ and $Cs_{1.33}Ti_8O_{16}$. This was borne out of preliminary specimens which were all single phase provided certain precautions were taken during the firing of the materials. In all the specimens the starting materials $Cs_2CO_3$, $BaCO_3$ and $TiO_2$ were all pre-dried. After being weighed out the starting materials were mixed by wet milling with petroleum spirit in an agate ball mill for 30 min and then vacuum dried in a dessicator for over 2 h. The mixture was then compacted into a disc and calcined at 925 K in air for 1 h; if higher temperatures are used Cs becomes volatile. The decrease in weight at this stage agreed within 0·5% of the value expected for $CO_2$ loss. Each specimen was then ground up and a calculated amount of the fine graphite powder blended in to act as the reducing agent for converting $Ti^{4+}$ to $Ti^{3+}$. The final firing was carried out on compacted specimens for 12 h using a reducing atmosphere of 5% $H_2$ in $N_2$. The pure Cs hollandite was fired at 1440 K whilst the other two were fired at 1490 K and in each case the specimens were cooled to room temperature over a 12 to 16 h period. To prevent Cs loss at these temperatures each specimen was contained in an alumina crucible with a close-fitting lid which was clamped firmly against the ground crucible rim during firing. No significant change in the Ba/Ti and Cs/Ti ratio before and after firing was observed in any of the specimens according to an analysis of the Ba $L$, Cs $L$ and Ti $K$ X-ray fluorescence peaks recorded on a Philips XRF wavelength-dispersive spectrometer. All three specimens were single-phase tetragonal hollandites with well resolved X-ray powder diffraction peaks with no detectable impurity or superlattice lines in a continuous scan at $0{\cdot}05^\circ\,s^{-1}$ over the range $2\theta = 10$–$65^\circ$ using Cu $K\alpha$ radiation.

Neutron powder diffraction data for all the samples were collected at $\lambda = 1{\cdot}59327$ Å over the angular range $2\theta = 0$–$160^\circ$ using the high-resolution diffractometer D2B at the Institut Laue–Langevin. A description of the calibration procedure used to evaluate $\lambda$ and the resolution obtained from this instrument are documented in Cheary (1990). The design and general characteristics of D2B are discussed in Hewat (1986). Each specimen was ground to a powder fine enough to pass easily through a 38 μm sieve and then loaded onto the diffractometer in a sealed thin-walled V can. Data were collected at 5, 100, 200 and 300 K for each specimen using a continuous flow He cryostat. A cryofurnace was used to collect an additional data set at 400 K from the pure Cs hollandite.

Rietveld refinement of the neutron data was carried out using the program developed by Wiles & Young (1981) and extensively modified by Howard & Hill (1986). In this analysis the profiles were modelled by a full Voigt function including an asymmetry term to represent the effects of vertical divergence (Howard, 1982). The data were corrected for zero error in the refinement and the background

was fitted to a function of the form $b_0 + b_1 2\theta + b_2 2\theta^2 + b_3/2\theta$. Close inspection of the diffraction data revealed a number of very weak unidentified diffraction lines in each of the specimens but these were excluded from the refinement. Even when included in the refinement these lines had negligible effect on the final results. The goodness-of-fit indicators quoted in the table of results are the weighted pattern $R$ factor $R_{wp}$, its expected value on the basis of counting statistics $R^E_{wp}$ and the Bragg $R$ factor $R_B$ as defined in Howard & Hill (1986).

All the patterns were refined in the space group $I4/m$ and convergence was achieved without problem. The refined atomic coordinates, lattice parameters and temperature factors for each recorded neutron pattern are given in Table 1 with the atomic coordinates described according to the scheme,

$A$-site ions in 4($e$): $00z$,
Ti and O in 8($h$): $uv0$ or $xy0$.

The compositions quoted in the table were obtained by refinement of the occupancy on the $A$ sites. As Ba and Cs possess similar scattering lengths an average value was adopted for the $A$ sites on the basis of the proportion of each ion in the preparation mixture; the $Ti^{3+}/Ti^{4+}$ ratio on the $B$ sites was calculated from the charge-balance equation once the total occupancy was known. In each case the observed occupancy on the $A$ sites was close to the value expected. Isotropic temperature factors were used for Ti and O, but anisotropic temperature factors were required for the $A$ ions to reflect positional disorder in the $c$ direction as in earlier refinements (Cheary, 1986; Sabine & Hewat, 1982). Corrections for absorption were applied to the temperature factors (Hewat, 1979) but in general the changes in $B$ were small (*i.e.* $\Delta B \simeq 0{\cdot}01$ Å$^2$). Very good fits were obtained to the patterns with $R_{wp}$ between 7 and 7·5% for $R^E_{wp} \simeq 2\%$. The structural parameters model the data well with $R_B$ down to 1·4% for the Cs hollandite and only rising to 2·8% at worst.

Table 1. *Structural parameters for the titanate hollandites* $Cs_{1.36}Ti_8O_{16}$, $Cs_{0.82}Ba_{0.41}Ti_8O_{16}$ *and* $Cs_{0.40}Ba_{0.79}Ti_8O_{16}$ *obtained by Rietveld refinement of high-resolution neutron powder diffraction data* ($\lambda$ = 1·59327 Å) *collected over the temperature range* 5 *to* 400 K

The e.s.d.'s given by the refinement are included in parentheses.

| | | 5 K | 100 K | 200 K | 300 K | 400 K |
|---|---|---|---|---|---|---|
| $Cs_{1.36\pm0.03}(Ti^{3+}_{1.36\pm0.03}Ti^{4+}_{6.64\pm0.03})O_{16}$ | | | | | | |
| $a$ (Å) | | 10·2682 (2) | 10·2705 (2) | 10·2766 (2) | 10·2846 (2) | 10·2947 (2) |
| $c$ (Å) | | 2·96433 (5) | 2·96469 (5) | 2·96600 (2) | 2·96810 (5) | 2·97087 (6) |
| Cs + Ba | $z$ | 0·371 (2) | 0·370 (2) | 0·374 (3) | 0·373 (3) | 0·376 (4) |
| | $\beta_{11}$ | 0·0003 (3) | 0·0006 (3) | 0·0011 (4) | 0·0017 (4) | 0·0028 (4) |
| | $\beta_{33}$ | 0·106 (12) | 0·113 (12) | 0·147 (17) | 0·148 (18) | 0·190 (3) |
| | $B$ (Å$^2$) | 1·39 (12) | 1·50 (13) | 2·03 (20) | 2·20 (20) | 3·02 (35) |
| Ti | $u$ | 0·3487 (2) | 0·3488 (2) | 0·3486 (2) | 0·3485 (2) | 0·3484 (2) |
| | $v$ | 0·1654 (2) | 0·1654 (2) | 0·1650 (2) | 0·1652 (3) | 0·1654 (3) |
| | $B$ (Å$^2$) | 0·50 (2) | 0·54 (3) | 0·65 (3) | 0·74 (2) | 0·79 (2) |
| O1 | $x$ | 0·1575 (2) | 0·1576 (2) | 0·1577 (2) | 0·1580 (2) | 0·1578 (2) |
| | $y$ | 0·2083 (1) | 0·2084 (1) | 0·2084 (1) | 0·2084 (1) | 0·2085 (1) |
| | $B$ (Å$^2$) | 0·48 (2) | 0·53 (2) | 0·59 (3) | 0·67 (3) | 0·74 (3) |
| O2 | $x$ | 0·5374 (1) | 0·5374 (1) | 0·5376 (2) | 0·5377 (1) | 0·5376 (2) |
| | $y$ | 0·1668 (2) | 0·1668 (2) | 0·1666 (2) | 0·1664 (2) | 0·1663 (2) |
| | $B$ (Å$^2$) | 0·56 (3) | 0·59 (2) | 0·67 (3) | 0·81 (2) | 0·87 (2) |
| $R_{wp}$ (%) | | 7·1 | 7·1 | 7·2 | 7·2 | 7·2 |
| $R^{exp}_{wp}$ (%) | | 2·0 | 2·0 | 2·0 | 2·0 | 2·0 |
| $R_B$ (%) | | 1·4 | 1·5 | 1·6 | 1·6 | 1·6 |
| $Cs_{0.82}Ba_{0.41}(Ti^{3+}_{1.64\pm0.03}Ti^{4+}_{6.36\pm0.03})O_{16}$ | | | | | | |
| $a$ (Å) | | 10·2152 (2) | 10·2175 (2) | 10·2223 (2) | 10·2289 (2) | - |
| $c$ (Å) | | 2·96094 (5) | 2·96180 (5) | 2·96374 (2) | 2·96633 (5) | - |
| Cs + Ba | $z$ | 0·385 (2) | 0·381 (2) | 0·382 (2) | 0·381 (2) | - |
| | $\beta_{11}$ | 0·0001 (4) | 0·0004 (4) | 0·0009 (4) | 0·0014 (5) | - |
| | $\beta_{33}$ | 0·069 (10) | 0·077 (10) | 0·124 (14) | 0·122 (14) | - |
| | $B$ (Å$^2$) | 0·82 (11) | 1·10 (12) | 1·70 (16) | 1·83 (16) | - |
| Ti | $u$ | 0·3493 (2) | 0·3490 (2) | 0·3490 (2) | 0·3491 (2) | - |
| | $v$ | 0·1660 (2) | 0·1657 (2) | 0·1654 (2) | 0·1655 (2) | - |
| | $B$ (Å$^2$) | 0·58 (3) | 0·62 (3) | 0·63 (2) | 0·85 (2) | - |
| O1 | $x$ | 0·1571 (2) | 0·1572 (2) | 0·1575 (2) | 0·1573 (2) | - |
| | $y$ | 0·2051 (1) | 0·2053 (1) | 0·2055 (1) | 0·2055 (1) | - |
| | $B$ (Å$^2$) | 0·52 (2) | 0·56 (3) | 0·54 (2) | 0·72 (3) | - |
| O2 | $x$ | 0·5388 (1) | 0·5385 (1) | 0·5388 (1) | 0·5386 (1) | - |
| | $y$ | 0·1671 (2) | 0·1675 (2) | 0·1674 (2) | 0·1673 (2) | - |
| | $B$ (Å$^2$) | 0·55 (3) | 0·55 (2) | 0·64 (3) | 0·80 (3) | - |
| $R_{wp}$ (%) | | 7·6 | 7·4 | 7·0 | 7·1 | - |
| $R^{exp}_{wp}$ (%) | | 2·1 | 2·1 | 2·1 | 2·1 | - |
| $R_B$ (%) | | 2·8 | 2·8 | 2·3 | 2·6 | - |
| $Cs_{0.40}Ba_{0.79}(Ti^{3+}_{1.99\pm0.03}Ti^{4+}_{6.01\pm0.03})O_{16}$ | | | | | | |
| $a$ (Å) | | 10·1688 (2) | 10·1716 (2) | 10·1764 (2) | 10·1830 (2) | - |
| $c$ (Å) | | 2·95945 (5) | 2·96028 (5) | 2·96260 (2) | 2·96538 (5) | - |
| Cs + Ba | $z$ | 0·402 (2) | 0·399 (3) | 0·400 (3) | 0·399 (3) | - |
| | $\beta_{11}$ | 0·0005 (5) | 0·0010 (4) | 0·0019 (4) | 0·0027 (4) | - |
| | $\beta_{33}$ | 0·069 (10) | 0·077 (10) | 0·124 (14) | 0·122 (14) | - |
| | $B$ (Å$^2$) | 1·20 (20) | 1·68 (20) | 2·03 (23) | 2·34 (25) | - |
| Ti | $u$ | 0·3502 (2) | 0·3503 (2) | 0·3502 (2) | 0·3503 (2) | - |
| | $v$ | 0·1670 (2) | 0·1668 (2) | 0·1667 (2) | 0·1664 (2) | - |
| | $B$ (Å$^2$) | 0·58 (2) | 0·62 (2) | 0·67 (2) | 0·76 (2) | - |
| O1 | $x$ | 0·1561 (2) | 0·1562 (2) | 0·1562 (2) | 0·1562 (2) | - |
| | $y$ | 0·2021 (1) | 0·2022 (1) | 0·2024 (1) | 0·2025 (1) | - |
| | $B$ (Å$^2$) | 0·48 (2) | 0·52 (2) | 0·59 (2) | 0·68 (2) | - |
| O2 | $x$ | 0·5392 (1) | 0·5391 (1) | 0·5391 (1) | 0·5391 (1) | - |
| | $y$ | 0·1669 (2) | 0·1669 (2) | 0·1669 (2) | 0·1669 (2) | - |
| | $B$ (Å$^2$) | 0·51 (3) | 0·56 (2) | 0·63 (2) | 0·77 (2) | - |
| $R_{wp}$ (%) | | 7·5 | 7·4 | 7·4 | 7·4 | - |
| $R^{exp}_{wp}$ (%) | | 2·2 | 2·2 | 2·2 | 2·1 | - |
| $R_B$ (%) | | 2·3 | 2·2 | 2·1 | 2·1 | - |

## Analysis and discussion of results

The absolute values of the refined $A$-site occupancies are within 0·04 ions per cell of the intended values. As expected the occupancy increases uniformly with Cs concentration although the relationship is not exactly linear. The lattice parameters, $a$ and $c$, for each compound are well behaved with temperature $T$ fitting closely to the relation

$$a \text{ (or } c) = a_0 + a_2T^2 + a_3T^3 \ (T \text{ in K}). \qquad (1)$$

Although both $a$ and $c$ increase as more Cs is concentrated into the tunnels they seem to be controlled in slightly different ways. In particular $a_0$, the lattice parameter at 0 K, is distinctly linear when plotted against the Cs content but displays some irregularity when plotted against the total occupancy on the $A$ sites. With $c_0$ the situation is reversed;

linearity is produced by plotting against the total occupancy on the $A$ sites. The plots for $a_0$ and $c_0$ are shown along with the lines of best fit in Figs. 2(*a*,*b*). To show the behaviour over the whole composition range, these figures along with later figures include results for the metastable tetragonal end-member hollandite $Ba_{1\cdot07}Ti_8O_{16}$ (Cheary, 1990). At room temperature (300 K) the expansion in the present samples becomes isotropic when all the Ba has been replaced by Cs. In $Ba_{1\cdot07}$ hollandite the expansion coefficient $\alpha_c$ along the tunnel axis, given by $(1/c)(dc/dT)$, is $14 \times 10^{-6}\,K^{-1}$ and double the expansion coefficient $\alpha_a$ in the $a$ direction given by $(1/a)(da/dT)$. The expansion coefficients merge to a value of $\sim 8 \times 10^{-6}\,K^{-1}$ in $Cs_{1\cdot36}Ti_8O_{16}$ which is similar to the value $11 \times 10^{-6}\,K^{-1}$ obtained by Sabine & Hewat (1982) for $Ba_{1\cdot14}(Al_{2\cdot28}Ti_{5\cdot72})O_{16}$. A plot of $\alpha_a$ and $\alpha_c$ as a function of the Cs content per cell is given in Fig. 2(*c*).

When Cs is substituted into Ba hollandite the tunnel site it occupies is intrinsically smaller than the ion itself. The Cs—O bond length is typically > 3·1 Å (Shannon, 1976) but in $Ba_{1\cdot07}Ti_8O_{16}$ the Ba—O distance averaged over the eight O1 oxygens forming the tunnel cavity is 2·94 Å at 5 K. Also the distance between the centres of adjacent tunnel cavities along the tunnel axis, namely the $c$ parameter, is only slightly larger at 2·956 Å. To accommodate Cs the box of oxygens needs to be enlarged but this can only occur by deformation of the oxygen octahedra in the tunnel walls. Two factors control the size and shape of these oxygen octahedra; the amount of Cs in the tunnels and the relative concentration of $Ti^{3+}$ and $Ti^{4+}$ in the octahedra. As the Cs concentration increases the proportion of $Ti^{3+}$ ions on the $B$ sites decreases and up to ~0·8 Cs per cell the mean ⟨Ti—O⟩ bond length also decreases. Beyond this level the ⟨Ti—O⟩ length undergoes an anomalous increase as shown in Fig. 3(*a*). When Cs is absent the ⟨Ti—O⟩ bond length is determined primarily by the $Ti^{3+}/Ti^{4+}$ ratio and the Ba ion in the tunnel has little influence (Post, von Dreele & Buseck, 1982). However, as the Cs level increases, the centres of the walls are compressed by the presence of these ions on either side of the wall and the wall thickness decreases at its centre. In $Cs_{1\cdot36}Ti_8O_{16}$ the oxygens

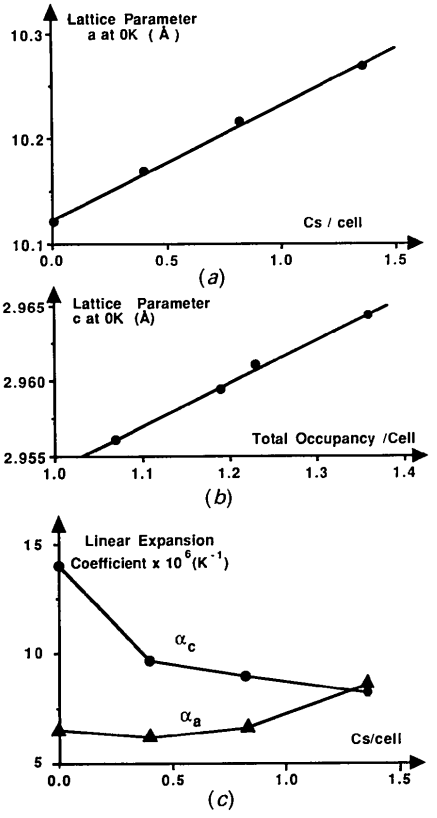


Fig. 2. Lattice parameters (*a*) $a$ and (*b*) $c$ for $Cs_{1\cdot36}Ti_8O_{16}$, $Cs_{0\cdot82}Ba_{0\cdot41}Ti_8O_{16}$ and $Cs_{0\cdot40}Ba_{0\cdot79}Ti_8O_{16}$ at 0 K as a function of the Cs content per unit cell, along with (*c*) the linear-expansion coefficients $\alpha_a = (1/a)(da/dT)$ and $\alpha_c = (1/c)(dc/dT)$ at 300 K. In these plots the error bars are encompassed by the plotting symbols.

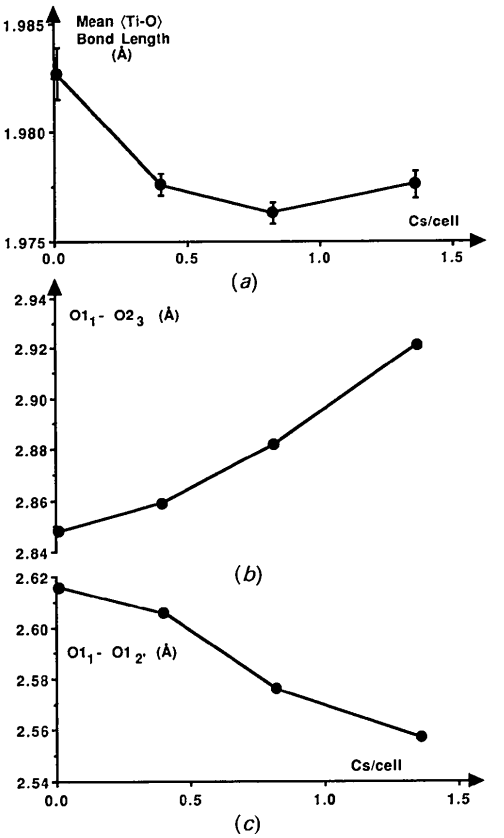


Fig. 3. The effect of Cs content on (*a*) the mean Ti—O bond length within the oxygen octahedra, (*b*) the separation of the oxygens $O1_1$—$O2_3$, a measure of the lateral dimensions of the tunnel walls, and (*c*) the separation of the oxygens $O1_1$—$O1_{2'}$, a measure of the thickness of the tunnel walls at the centre.

$O1_1$ and $O1_{2'}$ at the centre of each wall are only separated by ~2·55 Å and are clearly in intimate contact. At the same time the tunnel cross section is enlarged because the tunnel walls are also stretched laterally by the Cs ions. These effects are illustrated in Figs. 3(*b*,*c*) which show the effect of Cs on the $O1_1$—$O2_3$ separation, a measure of the lateral dimensions of the tunnel walls, and the $O1_1$—$O1_{2'}$ separation. In the O octahedra these two O—O separations are the only ones that change by more than 0·02 Å between end-member compounds.

The pressure imposed on the tunnel walls by Cs is also reflected in the thermal expansion of the oxygen octahedra in the walls relative to the tunnel volume between 5 and 300 K. Fig. 4 shows plots of the oxygen octahedral volume and the volume of the oxygen box or tunnel cavity surrounding each *A* site for each of the Cs-substituted hollandites over the temperature range 5 to 300 K. Over this temperature range the tunnel cavity volume increases linearly by 0·8% in each of the hollandites, but the expansion of the oxygen octahedra is smaller and dependent on the Cs content; 0·18% in $Cs_{1\cdot36}Ti_8O_{16}$ and 0·31% in $Cs_{0\cdot4}Ba_{0\cdot79}Ti_8O_{16}$. Reducing the proportion of Cs, therefore, allows the oxygen octahedra to expand more freely with temperature.

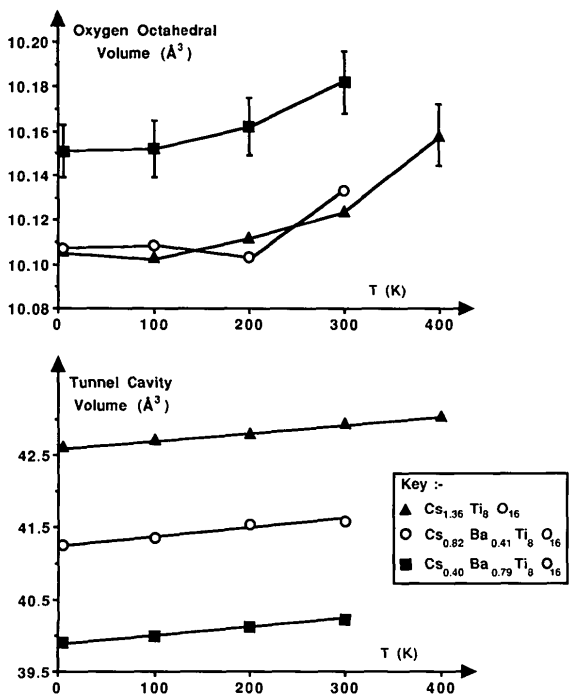


Fig. 4. The effect of temperature on the volume of the oxygen octahedra and the volume of the tunnel cavity around each tunnel site in $Cs_{1\cdot36}Ti_8O_{16}$, $Cs_{0\cdot82}Ba_{0\cdot41}Ti_8O_{16}$ and $Cs_{0\cdot40}Ba_{0\cdot79}Ti_8O_{16}$. The tunnel-cavity volume rises linearly with temperature and the slope is the same for each hollandite. The errors are similar for all the octahedral volume data but are omitted in some instances for clarity of presentation. The error bars for the tunnel-cavity data are smaller than the plotting symbols.

Fig. 4 shows clearly that Cs enlarges the tunnel site quite significantly. At 5 K the *A*-site tunnel volume in the $Cs_{1\cdot36}$ hollandite is approximately 10% larger than in the $Ba_{1\cdot07}$ hollandite and over the same range the mean $\langle A$—O$\rangle$ bond length increases from 2·95 to 3·07 Å. Despite the large size of Cs, these ions still appear to occupy an off-centre position within the *A*-site oxygen box. In $Cs_{1\cdot36}$ hollandite off-centring gives a short *A*—O bond length of 2·898 Å and a long *A*—O bond length of 3·266 Å. The magnitude of this short bond length is physically unrealistic for a Cs—O bond which is normally in excess of 3·10 Å. Presumably in this hollandite there is some degree of short-range ordering of the Cs along the tunnels with the filled and empty *A* sites closely following the 3*c* superstructure Cs—Cs—*V*—Cs—Cs—*V* (Kesson & White, 1986*a*,*b*) where *V* corresponds to a vacant *A* site. As the *c* parameter of the Cs hollandite is only 2·97 Å at room temperature and $Cs^+$ has a diameter of approximately 3·5 Å (Shannon, 1976) the oxygen box encompassing each occupied *A* site will be enlarged as mentioned earlier. To compensate for this the empty *A*-site cavities will be smaller than average. On any particular *A* site the Cs ion will be in contact with its eight surrounding oxygens and centrally located within its oxygen box. Relative to the lattice, however, a pair of caesiums in contact with each other in adjacent tunnel sites will occupy complementary off-centre positions. In $Cs_{1\cdot36}Ti_8O_{16}$ at 5 K, for instance, these positions correspond to $z = 0\cdot371$ and 0·629. In the two Cs/Ba hollandites analyzed the total occupancy is close to 1·2 ions per cell and at this level the appropriate superstructure of filled (*F*) and vacant (*V*) sites on the *A* sites is a 5*c* supercell (Bursill & Grzinic, 1980) of the type *F*—*F*—*V*—*F*—*V* where in this case *F* is either Ba or Cs. In $Cs_{0\cdot82}Ba_{0\cdot41}Ti_8O_{16}$ the Cs will probably occupy the *A* site with vacancies either side, and the superstructure will be either Cs—Ba—*V*—Cs—*V* or Ba—Cs—*V*—Cs—*V* depending on which configuration has the lowest energy. In $Cs_{0\cdot40}Ba_{0\cdot79}Ti_8O_{16}$ the Ba will probably be paired giving the superstructure Ba—Ba—*V*—Cs—*V*. This change in superstructure with Cs concentration is reflected by the average off-centre shift of the *A* ions which drops from 0·38 Å in $Cs_{1\cdot36}Ti_8O_{16}$ at 5 K to 0·29 Å in $Cs_{0\cdot40}Ba_{0\cdot79}Ti_8O_{16}$ at the same temperature.

The absence of superlattice lines in both the X-ray and neutron patterns indicates that ordering in the Cs hollandite and the other two Cs/Ba hollandites is only short range, possibly only a few cell lengths in extent. Over large distances the Cs, Ba and vacant sites will appear disordered on the tunnel sites as will the $Ti^{3+}$ and $Ti^{4+}$ amongst the *B* sites. In many previous refinements of hollandites the temperature

factors obtained have been larger than expected on the basis of thermal vibrations alone, particularly the anisotropic temperature factor $\beta_{33}$ representing the amplitude of vibration of the $A$-site ions in the direction of the tunnel axis [see for instance Sabine & Hewat (1982) or Cheary & Squadrito (1989)]. It would appear that a significant part of the observed temperature factors arises from static positional disorder of the $A$-site ions and the $B$ ions about their mean atomic coordinates. The existence of a static disorder term in the present temperature factors can be demonstrated by assuming the thermal part of the temperature factor is given by a Debye model. In multi-atom unit cells this model does not allow individual temperature factors to be calculated, but it does allow the average mass-weighted temperature factor per unit cell $B_M$ to be calculated. This is given by

$$B_M = \frac{1}{M}\sum_i^{\text{cell}} m_i B_i \tag{2}$$

where $B_i$ is the temperature factor of the $i$th atom in the unit cell, $m_i$ is the atomic mass of the $i$th atom and $M = \sum m_i$ is the total atomic mass of the unit cell. According to Blackman (1956) the thermal part of $B_M$, termed $B_M^{\text{thermal}}$ is given by

$$B_M^{\text{thermal}} = \frac{6gh^2}{Mk\theta_M}\left[\frac{\varphi(x)}{x} + \frac{1}{4}\right] \tag{3}$$

where $g$ is the number of atoms per cell, $h$ is Planck's constant, $k$ is Boltzmann's constant, $\theta_M$ is the Debye temperature and $\varphi(x)$ is the Debye function defined by

$$\varphi(x) = \frac{1}{x}\int_0^x \frac{\zeta \mathrm{d}\zeta}{\mathrm{e}^\zeta - 1}$$

where $x = \theta_M/T$. When the static disorder component $B_M^{\text{static}}$ is included, the total $B_M$ will be given by

$$B_M = B_M^{\text{thermal}} + B_M^{\text{static}}. \tag{4}$$

The measured values of $B_M$ for the present samples, obtained by averaging the individual temperature factors for Ba/Cs, Ti and O according to equation (2), are plotted in Fig. 5. The curves included in these plots are calculated thermal values for $B_M$ from the Debye expression [equation (3)] superimposed on a temperature-independent term $B_M^{\text{static}}$. All three of the Cs/Ba hollandites possess a Debye temperature $\theta_M$ in the range 420 to 460 K which corresponds to a thermal $B_M$ at 0 K of approximately 0·2 Å$^2$. The static contribution to $B_M$ in each case is between 0·4 and 0·5 Å$^2$ giving an isotropic r.m.s. displacement averaged over all atoms in a unit cell, $\langle u\rangle = (B_M/8\pi^2)^{1/2}$ between 0·07 and 0·08 Å.

An estimate of the static contribution to the individual temperature factors can be obtained using an approach developed by Housley & Hess (1966) which is outlined below. For harmonic vibrations the value of $B$ for an individual atom at 0 K, $B_i(0)$, is given by,

$$B_i(0) = h/m_i\nu_i(-1) \tag{5}$$

where $m_i$ is the mass of the $i$th atom and $\nu_i(-1)$ is the mean weighted frequency based on the average of $1/\nu$. On the basis of the Thirring expansion the temperature factor $B_i(T)$ of the $i$th atom at any temperature $T$ satisfies the inequality,

$$B_i(T) \geq 2kT/m_i\nu_i^2(-2), \tag{6}$$

where $\nu_i(-2)$ is the mean weighted frequency based on the average of $1/\nu^2$. At high temperatures equation (6) is an equality. Assuming that $\nu_i(-1) \geq \nu_i(-2)$ a further inequality can be set up which gives the maximum thermal value for $B_i(0)$ in terms of $B_i(T)$ namely,

$$B_i^2(0) \leq h^2 B_i(T)/2m_i kT. \tag{7}$$

The right-hand side of this equation sets the maximum possible value for the thermal contribution to $B_i(0)$. Therefore, given an experimental temperature factor $B_i^{\text{exp}}(0)$ measured close to 0 K

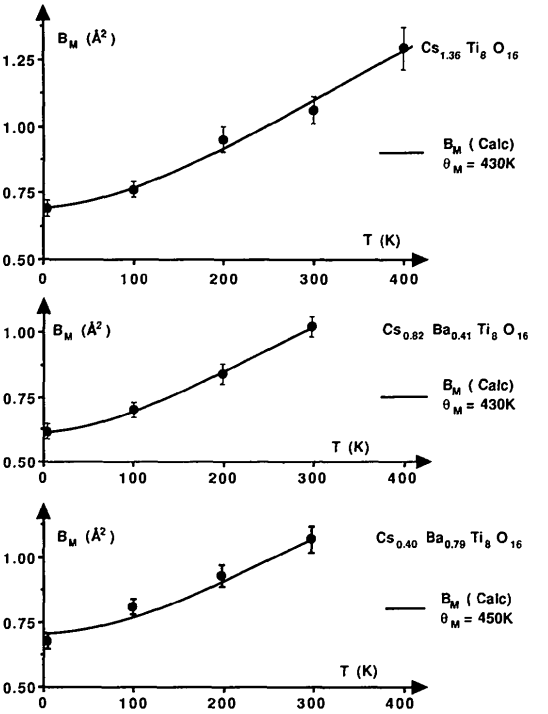


Fig. 5. Mass-weighted temperature factors $B_M$ for each hollandite as a function of temperature fitted with a Debye equation [equation (3)] plus a temperature-independent term, $B_M^{\text{static}}$, over the measured temperature range.

Table 2. *X-ray Debye temperatures* [$\theta_M$ (K)] *for titanate hollandites* $Cs_{1\cdot36}Ti_8O_{16}$, $Cs_{0\cdot82}Ba_{0\cdot41}Ti_8O_{16}$ *and* $Cs_{0\cdot40}Ba_{0\cdot79}Ti_8O_{16}$ *along with the maximum thermal contributions and the minimum static disorder contributions to the temperature factors*

| | $Cs_{1\cdot36}Ti_8O_{16}$ 430 (20) K | $Cs_{0\cdot82}Ba_{0\cdot41}Ti_8O_{16}$ 430 (15) K | $Cs_{0\cdot40}Ba_{0\cdot79}Ti_8O_{16}$ 450 (20) K |
|---|---|---|---|
| Cs + Ba | | | |
| Max. $\beta_{33}(0)$ thermal | 0·008 (2) | 0·008 (2) | 0·008 (1) |
| Min. $\beta_{33}(0)$ static | 0·098 (12) | 0·061 (13) | 0·083 (16) |
| Min. r.m.s. $u(0)$ (Å) | 0·21 (1) | 0·16 (2) | 0·19 (2) |
| Max. $\beta_{11}(0)$ thermal | 0·00031 (3) | 0·00028 (2) | 0·00040 (1) |
| Min. $\beta_{11}(0)$ static | 0 | 0 | 0 |
| Ti | | | |
| Max. $B(0)$ thermal (Å$^2$) | 0·17 (2) | 0·19 (2) | 0·19 (2) |
| Min. $B(0)$ static (Å$^2$) | 0·33 (3) | 0·39 (4) | 0·39 (3) |
| Min. r.m.s. $u(0)$ (Å) | 0·065 (3) | 0·070 (4) | 0·070 (3) |
| O1 | | | |
| Max. $B(0)$ thermal (Å$^2$) | 0·25 (1) | 0·30 (3) | 0·28 (2) |
| Min. $B(0)$ static (Å$^2$) | 0·23 (2) | 0·22 (4) | 0·20 (3) |
| Min. r.m.s. $u(0)$ (Å) | 0·054 (2) | 0·053 (4) | 0·050 (4) |
| O2 | | | |
| Max. $B(0)$ thermal (Å$^2$) | 0·28 (3) | 0·28 (2) | 0·30 (1) |
| Min. $B(0)$ static (Å$^2$) | 0·28 (4) | 0·20 (3) | 0·21 (3) |
| Min. r.m.s. $u(0)$ (Å) | 0·060 (4) | 0·050 (4) | 0·052 (3) |

(*i.e.* at 5 K) and a maximum thermal contribution of $B_i^{\text{thermal}}(0)_{\max}$, the minimum value for the static disorder contribution $B_i^{\text{static}}(0)_{\min}$ can be determined from the difference,

$$B_i^{\text{static}}(0)_{\min} = B_i^{\text{exp}}(0) - B_i^{\text{thermal}}(0)_{\max}. \quad (8)$$

Of particular interest to the present problem is the static contribution to the anisotropic temperature factor $\beta_{33}$ representing the r.m.s. displacement of the Cs and Ba along the tunnel axis. When expressed in terms of $\beta_{33}$ for a tetragonal hollandite, equation (7) becomes

$$\beta_{33}^2(0) \leq h^2\beta_{33}(T)/8c^2kT, \quad (9)$$

where $c$ is the tunnel-axis lattice parameter. Table 2 lists the values for $B_i^{\text{static}}(0)_{\min}$, $B_i^{\text{thermal}}(0)_{\max}$ and the static r.m.s. displacement of the atoms about their mean positions for the O and Ti ions. Also included in this table are the equivalent $\beta_{11}$ and $\beta_{33}$ components for the tunnel ions and the corresponding static r.m.s. displacement in the tunnel-axis direction. As the maximum thermal contribution at 0 K obtained from $B_i(T)$ or $\beta_{ii}(T)$ [using equations (7) or (9)] decreases with the temperature $T$, each value quoted in Table 2 was obtained by extrapolating the individual $B_i^{\text{thermal}}(0)_{\max}$ or $\beta_{ii}^{\text{thermal}}(0)_{\max}$ values derived at each temperature to the condition $T = \infty$ by extending a plot against $1/T$ to $1/T = 0$. This gives a better estimate of the 0 K contribution as the static disorder contribution at very high temperatures will be a negligible part of the temperature factor and equations (7) and (9) will be close to equalities rather inequalities. It should be noted that the experimental temperature factors at 5 K were used to represent the 0 K values.

The results in Table 2 demonstrate quite clearly that positional or static disorder constitutes a significant proportion of the temperature factors of all the ions. Static disorder amongst Ti and O is similar and does not differ much from sample to sample. At room temperature it contributes approximately 30% to the measured $B$ factors of Ti and O with the corresponding static r.m.s. displacement in the range 0·05 to 0·07 Å. The effect is more prominent in the tunnel of ions but only along the tunnel-axis direction; the static contribution perpendicular to the tunnels is small and $\beta_{11}$ is determined by thermal vibrations. Along the tunnels the static r.m.s. displacement is large and $\geq$0·16 Å in all the samples. Given that there is only short-range order of the caesiums in $Cs_{1\cdot36}Ti_8O_{16}$ but the majority are paired along the tunnels, the observed static r.m.s. displacement of $\simeq$0·2 Å is consistent with adjacent Cs being $\sim$3·5 Å apart (*i.e.* one ionic diameter) for a $c$ parameter of 3·0 Å.

One final factor that needs to be addressed in the context of nuclear-waste disposal is the dynamic stability of Cs and Ba in these hollandites. Whether or not these ions can migrate along the tunnels will be determined by the size of the square-planar array of oxygens $O1_1$—$O1_4$—$O1_2$—$O1_3$. The space at the centre of these should not be large enough to allow Ba or Cs to pass through. This means that the diagonal distance $O1_1$—$O1_2$ should be $< 2 \times$ Ba—O or Cs—O bond lengths at all temperatures (*i.e.* $<$5·64 or 6·28 Å, respectively). Fig. 6 shows that the $O1_1$—$O1_2$ distance plotted against temperature for each of the Cs/Ba hollandites is always less than either of the threshold separations. On the basis of these plots the increase in the $O1_1$—$O1_2$ distance between 0 and 1000 K will be between 0·05–0·06 Å in each hollandite and as such no migration should occur even at temperatures well in excess of 1000 K.

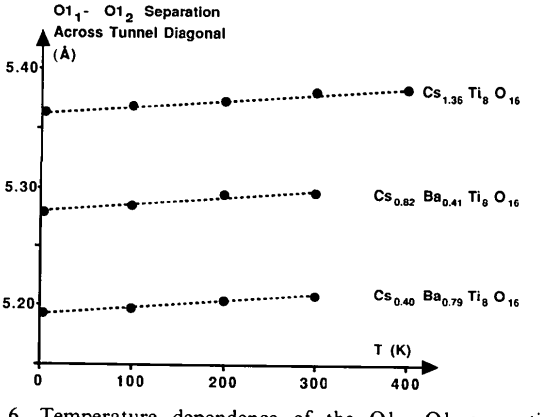


Fig. 6. Temperature dependence of the $O1_1$—$O1_2$ separation across the tunnel diagonal for each Cs/Ba hollandite. The variation is linear and the slope is almost the same in each case.

I wish to acknowledge the financial support given to this work by the Australian Nuclear Science and Technology Organisation under Research Contract No. 82/X/1. The neutron powder data for this work were collected at the Insitut Laue–Langevin, Grenoble, and I am indebted in particular to Dr Alan Hewat for providing access to the excellent facilities at this laboratory. Many thanks are extended to Joanne Hodge for assistance with the sample preparation.

### References

BLACKMAN, M. (1956). *Acta Cryst.* **9**, 734–737.
BURSILL, L. A. & GRZINIC, G. (1980). *Acta Cryst.* B**36**, 2902–2913.
CHEARY, R. W. (1986). *Acta Cryst.* B**42**, 229–236.
CHEARY, R. W. (1987). *Acta Cryst.* B**43**, 28–34.
CHEARY, R. W. (1988). *Mater. Sci. Forum*, **27**, 397–406.
CHEARY, R. W. (1990). *Acta Cryst.* B**46**, 599–609.
CHEARY, R. W. & SQUADRITO, R. (1989). *Acta Cryst.* B**45**, 205–212.
FIELDING, P. E. & WHITE, T. J. (1987). *J. Mater. Res.* **2**, 387–414.
HEWAT, A. (1979). *Acta Cryst.* A**35**, 248.
HEWAT, A. (1986). *Mater. Sci. Forum*, **9**, 69–80.
HOUSLEY, H. M. & HESS, F. (1966). *Phys. Rev.* **146**, 517–526.
HOWARD, C. J. (1982). *J. Appl. Cryst.* **15**, 615–620.
HOWARD, C. J. & HILL, R. J. (1986). Report AAEC/M112. Australian Atomic Energy Commission, Lucas Heights Research Laboratories, Australia.
KESSON, S. E. & WHITE, T. J. (1986*a*). *Proc. R. Soc. London Ser. A*, **405**, 73–101.
KESSON, S. E. & WHITE, T. J. (1986*b*). *Proc. R. Soc. London Ser. A*, **408**, 295–319.
POST, J. E., VON DREELE, R. B. & BUSECK, P. R. (1982). *Acta Cryst.* B**38**, 1056–1065.
ROTH, R. (1981). Annual Report NBSIR81-2241. National Measurements Laboratory, Office of Nuclear Technology, Australia.
SABINE, T. M. & HEWAT, A. (1982). *J. Nucl. Mater.* **110**, 173–177.
SHANNON, R. D. (1976). *Acta Cryst.* A**32**, 751–767.
WILES, D. B. & YOUNG, R. A. (1981). *J. Appl. Cryst.* **14**, 149–150.

*Acta Cryst.* (1991). B**47**, 333–337

# The Commensurate (10/4) Cluster Model in Quenched Wüstite $P''$. New Simulation of HREM Direct Images

BY G. NIHOUL

*GMET, Université de Toulon et du Var, BP* 132, 83957 *La Garde CEDEX, France*

J.-R. GAVARRI

*LCMPCT, Université de Toulon et du Var*, 83957 *La Garde CEDEX, France*

AND C. CAREL

*Laboratoire de Cristallochimie, Université de Rennes* I, 35042 *Rennes CEDEX, France*

(*Received* 24 *May* 1990; *accepted* 6 *December* 1990)

## Abstract

In the case of non-stoichiometric quenched wüstite $P''$ with the formula $Fe_{1-z}O$ ($z \simeq 0{\cdot}096$), the defect structure is shown to consist most probably of clusters composed of ten vacancies and four interstitial $Fe^{III}$ ions. These clusters are in agreement with a long-range ordering ($2{\cdot}5X$, $2{\cdot}5X$, $5X$), with some disorder in their local arrangement. The direct images of the quenched phase $P''$, previously obtained by various authors, are reinterpreted from a (10/4) cluster model: computer simulations have been carried out using this new model. The simulated images are in good agreement with the experimental images found in the literature.

## I. Introduction

In the Fe–O system, iron monoxide or wüstite shows a particularly large deviation from stoichiometry and a complex behavior under equilibrium conditions at high temperature (Vallet & Carel, 1989). This is why many previous structural studies (Koch & Cohen, 1969; Cheetham, Fender & Taylor, 1971; Catlow & Fender, 1975; Gavarri, Carel & Weigel, 1979; Gavarri, Carel, Jasienska & Janowski, 1981; Gartstein, Mason & Cohen, 1986) have been performed on this material at high temperature or after quenching. It has been shown that the wüstites are characterized by various types of clustering of vacancies (□) and interstitial $Fe^{III}$ ions occupying the octahedral (octa) and tetrahedral (tetra) sites respectively of the NaCl lattice with the general formula:

$$Fe_{1-z}O \equiv [Fe^{2+}]^{octa}_{1-3z}[Fe^{3+}]^{octa}_{2z-t}[Fe^{3+}]^{tetra}_{t}[\square]_{z+t}O^{2-}$$

In more recent studies (Gavarri *et al.*, 1979, Gartstein *et al.*, 1986; Gavarri & Carel, 1989; Carel & Gavarri, 1990), the ratio $R = (z + t)/t$ has been shown to be close to $2{\cdot}4 \pm 0{\cdot}4$ for quenched and

0108-7681/91/030333-05$03.00